Intramolecular Rearrangement Mechanisms in Five-Coordinate Complexes

P. Meakin,* E. L. Muetterties, and J. P. Jesson

Contribution No. 1891 from the Central Research Department, E. I. du Pont de Nemours and Company, Experimental Station, Wilmington, Delaware 19898. *Received December 10, 1971*

Abstract: Proposed mechanisms for intramolecular rearrangements are usually based on idealized coordination geometries, but such models often do not bear close correspondence to the geometries of systems which can be or have been studied experimentally. We report a case in point for a class of five-coordinate transition metal hydrides of the form HML_4 in which the geometry is neither trigonal bipyramidal nor square pyramidal. This class comprises the hydrides $HM(PF_3)_4$ (M = Co, Rh, Ir), $HM(PF_3)_4^-$ (M = Fe, Ru, Os), $HM[P(OC_2H_5)_3]_4$ (M = Co, Rh), and $HM[(C_6H_5)_2PCH_2CH_2P(C_6H_5)_2]_2$ (M = Rh, Ir). All members are stereochemically nonrigid on the nmr time scale and limiting slow and fast exchange spectra were observed for many of these hydrides. A new rearrangement mechanism is proposed on the basis of the actual ground-state geometry. In another stereochemically nonrigid class, $HIr(CO)_2(PR_3)_2$, the stereochemistry is such as to suggest an alternative to the idealized Berry rearrangement mechanism. The limitations of idealized rearrangement mechanisms are discussed and the probable multireaction path character of these rearrangements is emphasized. Nmr studies on molecules of the form $M(PF_3)_5$ (M = Fe, Ru, or Os) are also described. These molecules, unlike the $HM(PF_3)_4$ hydrides, ostensibly have the more common trigonal-bipyramidal ground-state form. Barriers to rearrangement appear to be very low.

Stereochemical nonrigidity is a ubiquitous feature of five-coordination. Mechanistic interpretation of rearrangements in five-coordinate molecules or ions has been based on a trigonal-bipyramidal (or square-pyramidal) ground state; this idealization, with the general assumptions of a Berry[1] rearrangement mechanism, has served to provide a consistent explanation for a large body of experimental data and to produce a model of substantial predictive value.[2] More recently other mechanisms have been outlined or proposed;[3-5] some advanced as alternatives to the Berry mechanism[4] and some proposed on the basis of ancilliary data.[5] We report here nuclear magnetic resonance data for several classes of stereochemically nonrigid five-coordinate transition metal complexes, especially hydrides of the type HML_4,[5] and propose rearrangement mechanisms which take explicit cognizance of the structural parameters and stereochemistries.

Experimental Section

Synthesis. All preparation and handling of the hydride complexes were effected in a dry nitrogen atmosphere (Vacuum Atmospheres Corp. Dri-Train). The following compounds were prepared by standard literature procedures: $M(PF_3)_5$[6] (M = Fe, Ru, Os), $H_2M(PF_3)_4$[6] (M = Fe, Ru, Os), $HM(PF_3)_4$[6] (M = Co, Rh, Ir), $HRh[(C_6H_5)_2PCH_2CH_2P(C_6H_5)_2]_2$,[7] $HIr[(C_6H_5)_2PCH_2CH_2P(C_6H_5)_2]_2$,[8] $HCo[P(OC_2H_5)_3]_4$,[9] $HNi[P(OC_2H_5)_3]_4^+X^-$,[10] and $HIr(CO)_2[P(C_6H_5)_3]_2$.[11] The anionic complexes, $HM(PF_3)_4^-$ (M = Fe, Ru, Os), were prepared in the nmr sample tube by adding 1 equiv of triethylamine to a solution of the corresponding $H_2M(PF_3)_4$ complex in $CHClF_2$ or acetone (d_6) at $-50°$. The hydride region nmr spectrum reported by Kruck and Prasch[6] for the $H_2Os(PF_3)_4$–$N(C_2H_5)_3$–acetone system cannot be assigned to $HOs(PF_3)_4^-$.

Chlorocarbonylbis(tri-*p*-tolylphosphine)iridium(I). Sodium chloroiridite (3.6 g, 0.095 mol) and 2-methoxyethanol (140 ml) were refluxed for 3.5 hr with carbon monoxide bubbling rapidly through the solution. The pale-yellow reaction mixture was then cooled to room temperature and pressure filtered with carbon monoxide. Tri-*p*-tolylphosphine (3.1 g, 0.0104 mol) was added to the resulting filtrate and the solution was stirred at 25° for 15 min again with carbon monoxide bubbling through the solution. The resulting slurry was heated to reflux for 30 min until all solids dissolved. The hot solution was pressure filtered with carbon monoxide and cooled slowly to room temperature and finally to 0°. The yellow crystals which formed were separated by filtration and washed with six 80-ml portions of petroleum ether. The crystals were air-dried in an oxygen-free drybox yielding 3.15 g of the desired product.

Anal. Calcd for $C_{43}H_{42}OClP_2Ir$: C, 59.74; H, 4.89. Found: C, 59.31, 58.92; H, 5.00, 5.18.

Hydridodicarbonylbis(tri-*p*-tolylphosphine)iridium(I). Chlorocarbonylbis(tri-*p*-tolylphosphine)iridium(I) (0.86 g, 0.001 mol) was added to 55 ml of carbon monoxide saturated ethanol. The resulting yellow slurry was heated to reflux while a vigorous stream of carbon monoxide was passed through the reaction mixture. Sodium borohydride (0.15 g, 0.004 mol) in 20 ml of ethanol was then added dropwise to the refluxing mixture and heating was continued for 30 min. The hot colorless solution was filtered in a carbon monoxide atmosphere and cooled slowly to −78° for 8 hr. The pale-yellow crystals which formed were separated by filtration, air-dried in an inert atmosphere, and then dissolved in a minimum of refluxing ethanol which was filtered and cooled to −78° for 8 hr. The resulting crystals were separated by filtration, washed with 20 ml of petroleum ether, and air-dried in an inert atmosphere for 24 hr. Hydridodicarbonylbis(tri-*p*-tolylphosphine)iridium is sensitive to oxygen and loses carbon monoxide under vacuum. The compound melts with decomposition at 176°. The infrared spectrum (Nujol) shows three strong bands at 1915, 1970, and 2080 cm^{-1}.

Anal. Calcd for $C_{44}H_{43}O_2P_2Ir$: C, 61.60; H, 5.05; O, 3.73. Found: C, 61.04; H, 5.14; O, 3.78.

Tetrakis(diethoxyphenylphosphine)rhodium Hydride. A mixture of rhodium trichloride trihydrate (5.2 g, 0.02 mol) and 50 ml of diethoxyphenylphosphine (excess) was gently heated until the reaction became exothermic. The reaction mixture was warmed to a gentle reflux for an additional 30 min until the mixture turned a deep yellow. Ethanol (150 ml) was added and to this sodium borohydride (2.0 g, 0.055 mol) was added very slowly in small portions. After refluxing for 30 min the mixture was cooled and then filtered. After removal of the ethanol by evaporation the

(1) R. S. Berry, *J. Chem. Phys.*, 32, 933 (1960).
(2) E. L. Muetterties, *Inorg. Chem.*, 4, 769 (1965); *Accounts Chem. Res.*, 3, 266 (1970); *Rec. Chem. Progr.*, 31, 51 (1970).
(3) E. L. Muetterties, *J. Amer. Chem. Soc.*, 91, 1636, 4115 (1969).
(4) I. Ugi, D. Marguarding, H. Klusacek, and P. Gillespie, *Accounts Chem. Res.*, 4, 288 (1971).
(5) P. Meakin, J. P. Jesson, F. N. Tebbe, and E. L. Muetterties, *J. Amer. Chem. Soc.*, 93, 1797 (1971).
(6) T. Kruck and A. Prasch, *Z. Anorg. Allg. Chem.*, 371, 1 (1969); T. Kruck, *Angew. Chem., Int. Ed. Engl.*, 6, 53 (1967).
(7) A. Sacco and R. Ugo, *J. Chem. Soc.*, 3274 (1964).
(8) R. A. Schunn, *Inorg. Chem.*, 9, 2567 (1970).
(9) W. Kruse and R. H. Atalla, *Chem. Commun.*, 921 (1968).
(10) C. A. Tolman, *J. Amer. Chem. Soc.*, 92, 4217 (1970).
(11) G. Yagupsky and G. Wilkinson, *J. Chem. Soc. A*, 725 (1969).

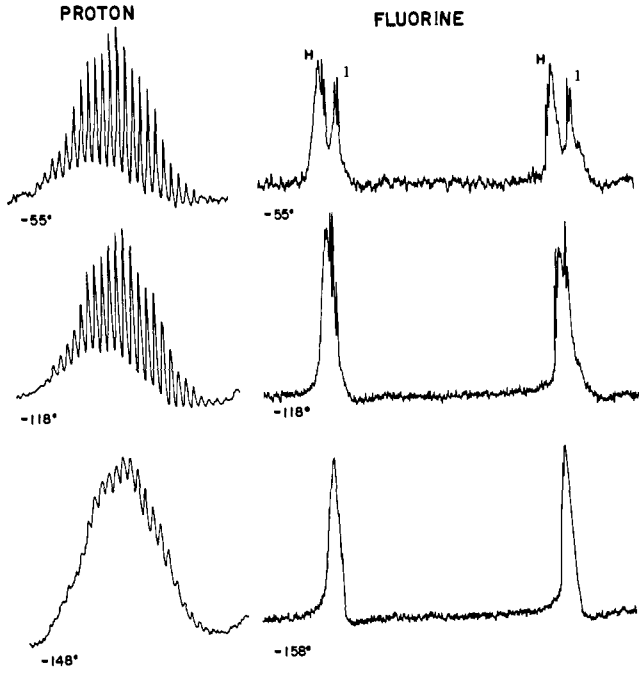

Figure 1. Temperature dependence of the ^1H (90 MHz) and ^{19}F (84.66 MHz) nmr spectra for $HFe(PF_3)_4^-$ in $CHClF_2$. H indicates the hydride ^{19}F resonances and I indicates the impurity $[Fe(PF_3)_5]$ ^{19}F resonances.

excess phosphine was recovered by heating *in vacuo* at 50°. Yellow solids were precipitated from the yellow oil with addition of petroleum ether (500 ml). The solids were separated by filtration and carefully washed with 400 ml of petroleum ether. The solids were dissolved in hot toluene (40–50 ml) which was then filtered and cooled to 5° to give tetrakis(diethoxyphenylphosphine)rhodium chloride.

Anal. Calcd for $C_{40}H_{60}O_8P_4RhCl$: C, 51.6; H, 6.49; Cl, 3.86. Found: C, 51.7; H, 6.49; Cl, 4.21.

Sodium borohydride (2.0 g, 0.055 mol) was added to an ethanolic solution (75 ml) of tetrakis(diethoxyphenylphosphine)rhodium chloride (3.84 g, 0.004 mol) and diethoxyphenylphosphine (0.99 g, 0.005 mol). The reaction mixture was gently refluxed in an argon atmosphere for 15 min and filtered hot. The pale yellow filtrate was cooled to −40° overnight and the resulting crystals were separated by filtration. The compound was recrystallized by dissolving in hot ethanol, filtering, and cooling the filtrate to −40°. The resulting chrome yellow crystals were separated by filtration and dried under vacuum for 2 hr at 50°. Tetrakis(diethoxyphenylphosphine)rhodium hydride is air sensitive and melts with decomposition at 173–174°; $\nu_{Rh-H} = 2000\ cm^{-1}$.

Anal. Calcd for $C_{40}H_{61}O_8P_3Rh$: C, 53.6; H, 6.85. Found: C, 53.2; H, 7.00.

Tris(triethyl phosphite)rhodium Hydride Dichloride. Rhodium trichloride trihydrate (5.2 g, 0.02 mol) and 25 ml of triethyl phosphite (excess) were slurried in a nitrogen atmosphere for 5 min and then gently heated until the reaction became exothermic. After 15 min the solution was cooled to 25° and filtered, and the excess phosphite was removed from the filtrate *in vacuo* at 80°. The resulting yellow oil was then extracted with petroleum ether (300 ml). The extracts were filtered and the filtrate was vacuum evaporated to an oil. The oil was again dried *in vacuo* at 80° for 8 hr. The yellow gum was recrystallized twice by dissolving in 100 ml of hot petroleum ether, filtering, and cooling slowly to −10° for 24 hr.

Anal. Calcd for $C_{18}H_{46}O_9P_3RhCl_2$: C, 32.1; H, 6.88; Cl, 10.5. Found: C, 30.6; H, 6.41; Cl, 10.6.

Tetrakis(triethyl phosphite)rhodium Hydride. Tris(triethyl phosphite)rhodium hydride dichloride (3.54 g, 0.005 mol) and triethyl phosphite (0.83 g, 0.055 mol) were slurried in ethanol in an argon atmosphere. Sodium borohydride (2.0 g, 0.055 mol) was added slowly and the solution was then gently refluxed for 30 min. The yellow solution was filtered and evaporated to dryness. The yellow gum was then extracted with petroleum ether (200 ml) and filtered, and the petroleum ether was removed *in vacuo*. The residue was recrystallized twice by dissolving in hot ethanol (20 ml), filtering, and cooling to −40° for 2 hr. The white needles that separated were collected and vacuum dried at 50° for 4 hr. Tetrakis(triethyl phosphite)rhodium hydride is air sensitive and melts with decomposition at 170–171°; $\nu_{Rh-H} = 1940\ cm^{-1}$.

Anal. Calcd for $C_{24}H_{61}O_{12}P_3Rh$: C, 37.5; H, 8.00. Found: C, 37.2; H, 7.96.

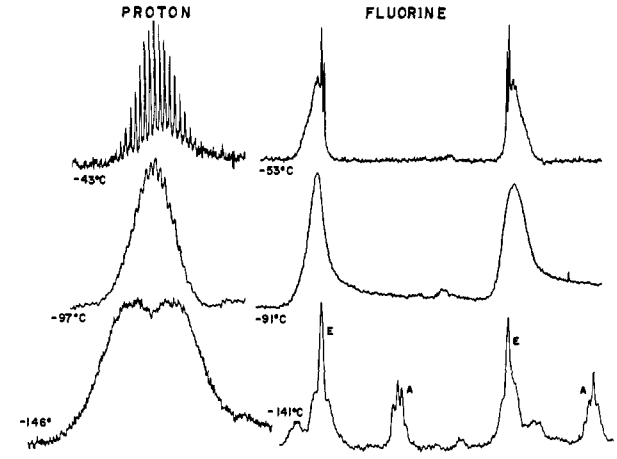

Figure 2. Temperature dependence of the ^1H (90 MHz) and ^{19}F (84.66 MHz) nmr spectra for $HRu(PF_3)_4^-$ in $CHClF_2$. A and E indicate axial and equatorial fluorine resonances.

Nmr Procedure and Analysis. ^1H and ^{19}F nmr spectra were measured on a Bruker HFX-90 spectrometer at 90 and 84.66 MHz, respectively. Temperatures were measured with a copper–constantan thermocouple located just beneath the spinning sample tube in the probe; this thermocouple was calibrated using a similar thermocouple held coaxially inside the spinning nmr sample tube which was partially filled with solvent. The nmr samples were prepared in a nitrogen atmosphere using deoxygenated solvents whenever possible. Chlorodifluoromethane and chlorodifluoromethane–methylene chloride mixtures were found to be very useful low-temperature solvents.

In those cases where a complete line-shape analysis was carried out, the density matrix approach of Kaplan[12] and Alexander[13] was employed. The details of such line-shape calculations have been presented in a recent paper.[14] Since the nmr spectra for which line-shape analyses are reported in this paper are first order, considerable simplifications are possible in the calculations. We have written general computer programs for both mutual and nonmutual intramolecular exchange processes in first-order systems. Exchange rates are obtained by a visual comparison of calculated and observed spectra.

Discussion

$HM(PF_3)_4$ Complexes. Nmr Data and Solution Structure. The ^{19}F (84.66 MHz) and ^1H (90 MHz) nmr spectra of $HFe(PF_3)_4^-$, $HRu(PF_3)_4^-$, $HCo(PF_3)_4$, and $HIr(PF_3)_4$ are shown in Figures 1–4 at three different temperatures; those for $HOs(PF_3)_4^-$ and $HRh(PF_3)_4$ were previously illustrated.[5]

These hydrides, except for the cobalt derivative, have a high-temperature limit proton nmr spectrum that consists of a tridecet of quintets with intensities in the proper binomial ratio, with additional fine structure due to ^1H–^{103}Rh coupling in the case of the rhodium complex. The averaged proton–fluorine coupling constant (15 Hz) is much larger than the proton–phosphorus coupling constant (3.75 Hz) for $HOs(PF_3)_4^-$; consequently the quintets are almost completely separated (see Figure 1 of ref 5). With extensive time averaging,

(12) J. I. Kaplan, *J. Chem. Phys.*, **28**, 278 (1958); **29**, 462 (1958).
(13) S. Alexander, *ibid.*, **37**, 967, 974 (1962); **38**, 1787 (1963); **40**, 2741 (1964).
(14) P. Meakin, E. L. Muetterties, F. N. Tebbe, and J. P. Jesson, *J. Amer. Chem. Soc.*, **93**, 4701 (1971).

Table I. Nmr Parameters for $HM(PF_3)_4$[a-c]

	$HFe(PF_3)_4^-$	$HRu(PF_3)_4^-$	$HOs(PF_3)_4^-$	$HCo(PF_3)_4$	$HRh(PF_3)_4$	$HIr(PF_3)_4$
			High-Temperature Limit			
$\|J_{HP}\|$	38.5	9.25	3.75	5.0	57.0	31.0
$\|J_{HF}\|$	9.6	16.5	15.0	9.75	16.5	14.75
$\|J_{HM}\|$					5.5	
$J_{FP} + 3J_{FP'}$	±1187	±1206	±1183	±1230	±1293	±1244
$J_{FP'}$ (min)	∓	∓	∓33	∓	∓	∓
δ_H	12.17	9.43	11.51	12.68	9.94	12.11
δ_F	−75.05	−77.9	−75.5	−64.7	−67.6	−57.6
			Low-Temperature Limit			
$\|J_{HP}\|_{trans}$		~75			215	170
$\delta_{F\ ax}$		−72.4	−69.5	−65.6	−63.7	−51.8
$\delta_{F\ eq}$		−78.5	−76.1	−63.7	−67.8	−57.5
$\Delta G^{\ddagger}$, kcal mol^{-1}	<5	7.0	8.0	5.5	9.0	10.0

[a] The proton chemical shifts in parts per million upfield from TMS. [b] ^{19}F chemical shifts are measured with respect to the upfield component of chlorodifluoromethane with the exception of $HIr(PF_3)_4$ where the shifts (ppm) are measured relative to 1,2-dibromotetrafluoroethane. Chlorodifluoromethane is 63.0 ppm upfield from trichlorofluoromethane and 1,2-dibromotetrafluoroethane is 72.1 ppm upfield from trichlorofluoromethane. [c] J values are in hertz.

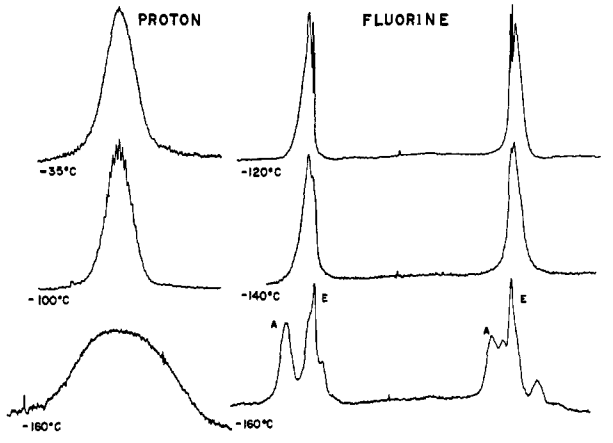

Figure 3. Temperature dependence of the ^1H (90 MHz) and ^{19}F (84.66 MHz) nmr spectra for $HCo(PF_3)_4$ in $CHClF_2$. A and E indicate axial and equatorial fluorine resonances.

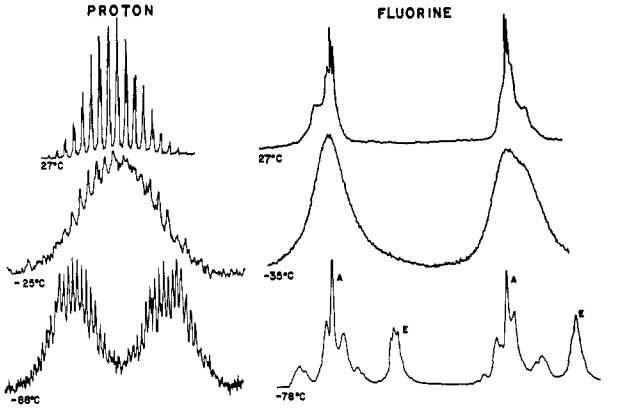

Figure 4. Temperature dependence of the ^1H (90 MHz) and ^{19}F (84.66 MHz) nmr spectra for $HIr(PF_3)_4$. The ^{19}F spectra were taken in CH_2Cl_2, the 27° ^1H spectrum in toluene-d_8, and the two low-temperature ^1H spectra in acetone-d_6. A and E indicate axial and equatorial fluorine resonances.

all 13 quintets in this complex were observed. These data indicate equivalence of the four PF_3 groups on the nmr time scale.

A complete analysis of the high-temperature limit ^{19}F nmr spectra was not made. However, calculations for similar but smaller spin systems of the type

$$A_nX\text{-}X'A_{n'} \text{ and } A_nX\text{-}X'(A_{n'})\text{-}X''A_{n''}$$

indicate that the high-temperature limit ^{19}F spectra for the complexes have an appearance consistent with a molecule containing four PF_3 groups equivalent on the nmr time scale. The spectra correspond to the A part of an $(A_3X)(A_3X)'(A_3X)''(A_3X)'''M$ spectrum with $J_{AX} = J_{A'X'} = J_{A''X''} = J_{A'''X'''} = J_{FP}$ = very large and with the other AX coupling constants ($J_{FP'}$, etc.) all equal, of much smaller magnitude than and of opposite sign to J_{FP}. The $AA'(FF')XX'(PP')$ coupling constants are also much smaller than J_{FP}. A further splitting is again observed in the case of $HRh(PF_3)_4$. The separation of the sharp doublets in the ^{19}F spectra is $|J_{FP} + 3J_{FP'}|$ and the doublet splitting is $|J_{FH}|$. For the case of $HRh(PF_3)_4$, $J_{FH} \approx J_{FRh}$ and two sharp triplets were observed.[5] This is the only information, apart from chemical shift data, that can be extracted directly from the ^{19}F high-temperature spectra without a complete analysis. However, if the FF′ and PP′ coupling constants are not too large, then the separation between the center of one of the sharp doublets (or triplets) and the center of intensity of the entire half of the ^{19}F spectrum of which that doublet is a part is approximately equal to $3J_{PF'}/2$. The value for $J_{PF'}$ obtained in this way represents a minimum value for this coupling constant and will be denoted as $J_{PF'}$ (min). Thus the high-temperature limit spectra establish the equivalence of the four PF_3 groups on the nmr time scale.

The proton nmr spectrum of $HCo(PF_3)_4$ is broad at room temperature (high-temperature limit; Figure 3) due to quadrupolar relaxation of the ^{59}Co nucleus of spin $I = {}^7/_2$, and the characteristic tridecet of quintets cannot be resolved. The ^{19}F spectrum seems to be unaffected by the quadrupolar relaxation probably because the ^{59}Co–^{19}F coupling constant is very small. In this case, equivalence of the four PF_3 groups on the nmr time scale at high temperature is established from the ^{19}F spectra alone. The high-temperature limit nmr parameters are given in Table I.

The ^{19}F nmr resonances of $HRu(PF_3)_4^-$, $HOs(PF_3)_4^-$, $HCo(PF_3)_4$, $HRh(PF_3)_4$, and $HIr(PF_3)_4$ broaden with decreasing temperature and at low temperatures appear as two complex, almost symmetrical patterns. These

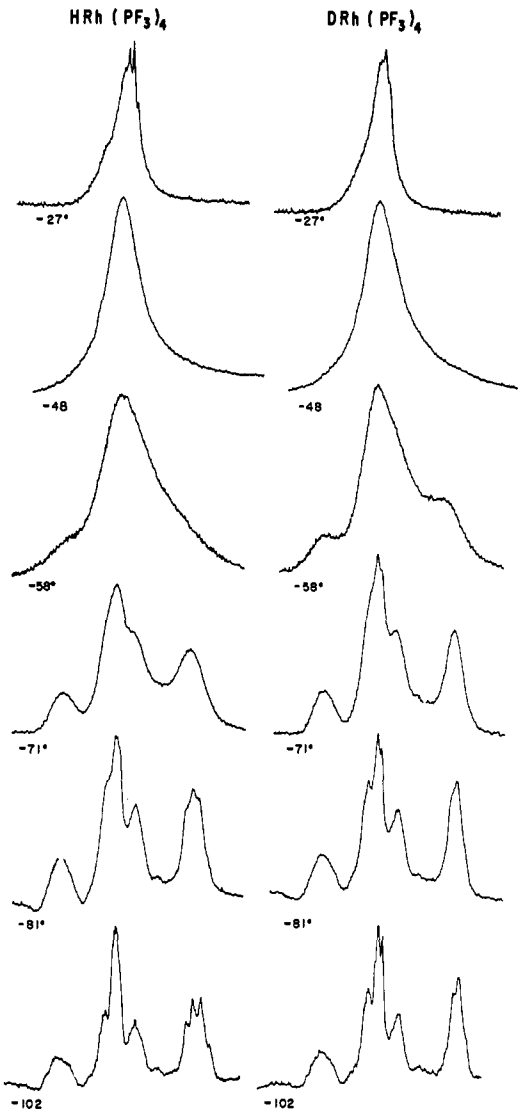

Figure 5. Temperature dependence of downfield half of the ^{19}F (84.66 MHz) nmr spectra for $HRh(PF_3)_4$ and $DRh(PF_3)_4$ in $CHClF_2$ taken at several temperatures between the slow and fast exchange limits.

complex sets which are well separated from each other and have relative integrated intensities in the ratio 1:3 establish a solution structure with one unique and three equivalent PF_3 groups. These data are consistent with a C_{3v} HMP_4 geometry similar to that found for the solid state structure from an X-ray crystal determination of $HCo(PF_3)_4$.[15] In the crystalline cobalt complex, the phosphorus nuclei are arranged about the cobalt nucleus in a near regular tetrahedral fashion with the hydrogen presumably on a tetrahedral face.

The low-temperature proton nmr spectrum of $HRu(PF_3)_4^-$, $HRh(PF_3)_4$, and $HIr(PF_3)_4$ can be described approximately as a complex doublet arising from the large trans H–P coupling[16] between the hydrogen and the axial (unique) ^{31}P nucleus. For $HCo(PF_3)_4$ (Figure 3) the main features of the temperature-dependent spectra are similar to those described above except that the temperature dependence of the proton spectra is further complicated by quadrupolar relaxation effects. The spectrum sharpens on cooling due to a lengthening of the rotational correlation time(s)[17] before it broadens due to the exchange process which is responsible for the temperature-dependent line shapes observed in the other $HM(PF_3)_4$ systems.[18] Nmr parameters obtained from the low-temperature spectra are shown in Table I.

The spectra for the anionic $HFe(PF_3)_4^-$ complex are somewhat different in that limiting slow exchange ^1H and ^{19}F spectra, analogous to those observed for the other $HM(PF_3)_4$ systems, were not obtained even at $-160°$. The spectra do broaden somewhat on cooling (Figure 1), but this broadening may reflect the effect of the increased viscosity of the solution at lower temperatures.

A complete density-matrix line-shape analysis is not feasible for the complex spin systems corresponding to the spectra of these $HM(PF_3)_4$ complexes. Indeed, the exact solution of the nmr eigenvalue problem corresponding to the low-temperature limit spectrum (an $A_3A_3'A_3''B_3MM'M''NX$ spin system) is in itself a formidable undertaking. It is possible, however, to obtain approximate exchange rates from an analysis of the ^{19}F spectra. This was accomplished by treating the line-shape effects observed in one half of the spectrum as an exchange between two sites with populations in the ratio 1:3. The complex structure observed in the low-temperature ^{19}F spectra is represented by using an appropriately broad line width at the two exchanging sites. Having obtained the exchange rate at one temperature in this manner, the free energy of activation at this temperature was obtained from the Eyring equation.[19] Assuming the transmission coefficient, K, to be equal to 1, the free energies of activation shown in Table I were obtained.

$$\text{rate}(T) = K(kt/h)e^{-\Delta G^{\pm}/RT}$$

For $HFe(PF_3)_4^-$ the observation that the four PF_3 groups are equivalent on the nmr time scale at all temperatures attainable in the $CHClF_2$ solvent used in these experiments could reflect a C_{4v} structure with four equivalent PF_3 groups or an intramolecular exchange process which is rapid on the nmr time scale even at $-160°$. The latter would require a free energy of activation of less than 5 kcal mol^{-1} for the exchange process. The trend toward lower barriers with decreasing atomic number and with decreasing formal charge observed in the five other complexes indicates that the barrier for $HFe(PF_3)_4^-$ may well be less than 5 kcal mol^{-1}. The five other $HM(PF_3)_4$ systems all have a C_{3v} HMP_4 framework, and we consider it highly unlikely that the iron analog would not be structurally analogous.

The ^{19}F spectra of $DRh(PF_3)_4$ have been measured over a range of temperatures (Figure 5) and compared

(15) B. A. Frenz and J. A. Ibers, *Inorg. Chem.*, **9**, 2403 (1970).

(16) B. L. Shaw and J. Chatt, *Abstr. Proc. Int. Conf. Coord. Chem.*, 7*th*, 293 (1962); J. Chatt, R. S. Coffey, and B. L. Shaw, *J. Chem. Soc.*, 7391 (1965).

(17) J. A. Pople, *Mol. Phys.*, **1**, 168 (1958); G. M. Whitesides and H. L. Mitchell, *J. Amer. Chem. Soc.*, **91**, 2245 (1969).

(18) There is no feature in the ^{19}F nor the ^1H nmr spectra of $HIr(PF_3)_4$ that can be attributed to either quadrupolar relaxation of the iridium nuclei or coupling to the iridium nuclei (^{191}Ir, 37.3%, $I = 3/2$; ^{193}Ir, 62.7%, $I = 3/2$). This could be due either to the small magnitude of the Ir–H and Ir–F coupling constants or to very rapid quadrupolar relaxation. Similarly for $HOs(PF_3)_4^-$ no effects were observed due to coupling to ^{189}Os (16.1%, $I = 3/2$); this may be due to the relatively small abundance of this isotope.

(19) W. P. K. Wynne-Jones and H. Eyring, *J. Chem. Phys.*, **3**, 492 (1935).

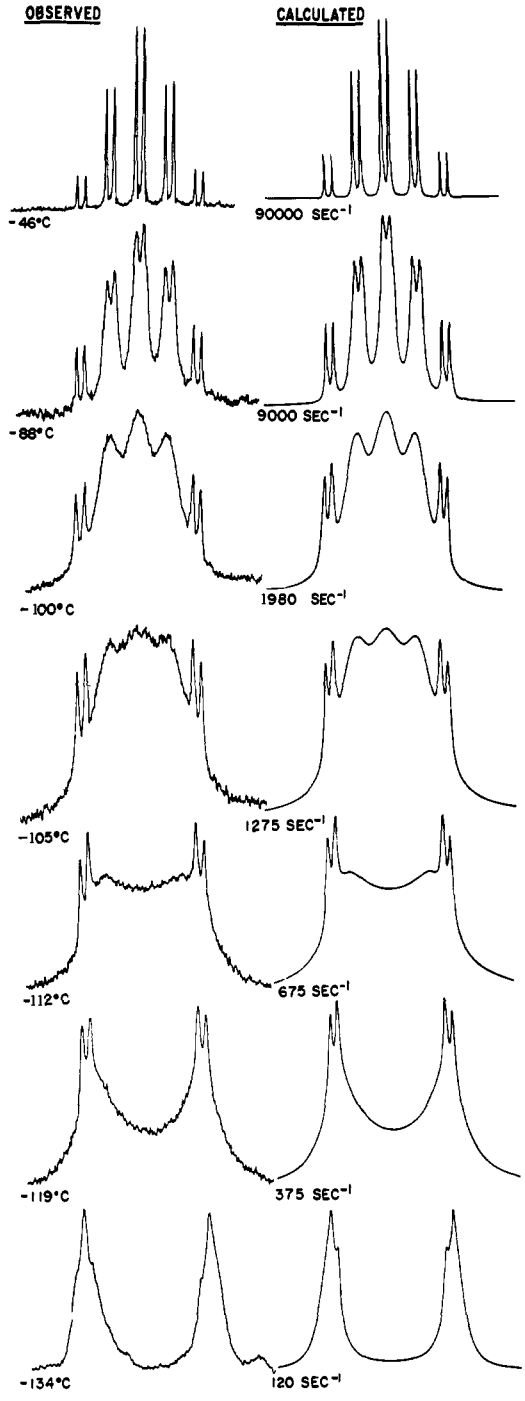

Figure 6. Observed and calculated hydride region ^1H (90 MHz) nmr spectra for $HRh[P(OC_2H_5)_3]_4$ in $CHClF_2$.

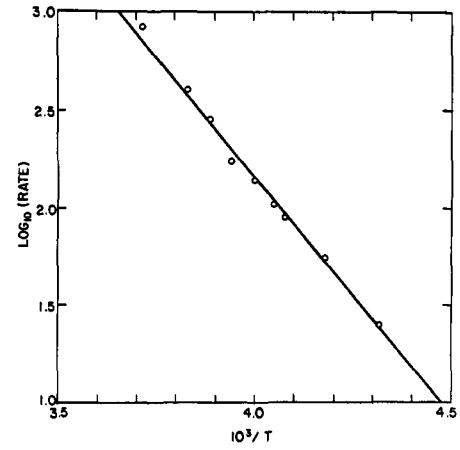

Figure 7. Arrhenius plot for the rate data obtained from the temperature-dependent hydride region ^1H (90 MHz) nmr spectra for $HRh[P(OC_2H_5)_3]_4$.

with the ^{19}F spectra of $HRh(PF_3)_4$ at the same temperatures. The complexity of the spectra precludes any quantitative comparison of the exchange rates. There does, however, seem to be a small isotope effect, with the exchange rates for $DRh(PF_3)_4$ being lower than those for $HRh(PF_3)_4$. The spectra of $HRh(PF_3)_4$ and $DRh(PF_3)_4$ were taken one after the other at the same temperature after the nmr probe had reached thermal equilibrium. The order in which they were measured was alternated, and spectra were taken at successively increasing and decreasing temperatures. A selection of these spectra is shown in Figure 5. The absolute temperatures may not be especially accurate, but the pairs of spectra in Figure 5 correspond to the same temperature to within 1°.

$HM(PR_3)_4$ Complexes. Nmr Data and Solution Structure. The temperature-dependent hydride region proton nmr spectra of a solution of $HRh[P(OC_2H_5)_3]_4$ in $CHClF_2$ taken over a temperature range of −46 to −134° are shown on the left-hand side of Figure 6. At −46°, the spectrum consists of a 1:4:6:4:1 quintet due to four equal ^1H–^{31}P couplings further split into doublets due to the ^1H–^{103}Rh coupling. The four phosphorus nuclei are thus equivalent on the nmr time scale. As the temperature is lowered, fairly complex nmr line-shape changes are observed. At −134°, the spectrum can crudely be described as a doublet due to the large trans ^1H–^{31}P coupling with the three other H–P couplings small. The −134° spectrum does not represent a low-temperature limit; on further cooling the spectrum broadens due to increasing viscosity, so that the low-temperature limit spectrum was not resolved. The −134° spectrum does, however, indicate a C_{3v} HMP_4 ground-state geometry. A permutational mechanistic analysis, of the type carried out for $H_2Fe[P(OC_2H_5)_3]_4$,[14] reveals that there can be only one type of temperature-dependent line-shape behavior for the C_{3v} case and that mechanistic information cannot be obtained from a jump model line-shape analysis (see Appendix I). The calculated line shapes in Figure 6 were obtained assuming a first-order low-temperature limit spectrum corresponding to a C_{3v} geometry with the nmr parameters $|J_{HRh}| = 9$ Hz, $J_{HP_{ax}} = \pm 152$ Hz, and $J_{HP_{eq}} = \mp 5$ Hz.

The spectra calculated from this model are in excellent agreement with the observed spectra (Figure 6); the resulting rate data are presented as an Arrhenius plot in Figure 7 and correspond to the rate expression

$$R(T) = 10^{10.4}e^{-5530/RT}$$

with the activation parameters

$$\Delta G^{\ddagger}(175°K) = 7.25 \text{ kcal mol}^{-1}$$

$$\Delta H^{\ddagger}(175°K) = 5.18 \text{ kcal mol}^{-1}$$

$$\Delta S^{\ddagger}(175°K) = -11.9 \text{ cal mol}^{-1} \text{ deg}^{-1}$$

The magnitude of the entropy of activation is larger than might be expected for a simple intramolecular re-

Table II. High-Temperature Limit Nmr Parameters and Upper Limits on the Free Energy of Activation for Mutual Exchange in Some Complexes of the Type HML_4[a]

Compound	Solvent	δ[b]	$\lvert J_{HP}\rvert_{av}$, Hz	$\lvert J_{HM}\rvert$, Hz	$\Delta G^{\ddagger}$, kcal mol^{-1}	Temp range, deg
$HRh[P(OC_2H_5)_3]_4$	$CHClF_2$	12.89	35	9	7.25	$-40 \rightarrow -150$
$HRh(diphos)_2$[c]	CD_2Cl_2	10.72	17.4	10.7	<7.5[f]	$+30 \rightarrow -110$
$HRh[P(OC_2H_5)_2C_6H_5]_4$[d]	Toluene-d_8	11.12	27.5	9.5	<8.5[f]	$+20 \rightarrow -50$
$HIr(diphos)_2$[e]	CD_2Cl_2	12.94	8.5		<7.5[f]	$+30 \rightarrow -110$
$HCo[P(OC_2H_5)_3]_4$	$CHClF_2$	15.47	19.5		<6.0[f]	$-40 \rightarrow -160$
$HNi[P(OC_2H_5)_3]_4^+$[e]	$CHClF_2$	14.09	26		<5.0[f]	$-40 \rightarrow -160$

[a] Spectra taken at 90 MHz on Bruker HFX-90 instrument. [b] Parts per million upfield from TMS. [c] diphos = $(C_6H_5)_2PCH_2CH_2P(C_6H_5)_2$. [d] Spectra taken at 220 MHz on Varian HR-220 instrument. The solubility is low. [e] $Ni[P(OC_2H_5)_3]_4 + CF_3COOH$: W. C. Drinkard, D. R. Eaton, J. P. Jesson, and R. V. Lindsey, Jr., *Inorg. Chem.*, **9**, 392 (1970). [f] Assuming a C_{3v} ground-state structure.

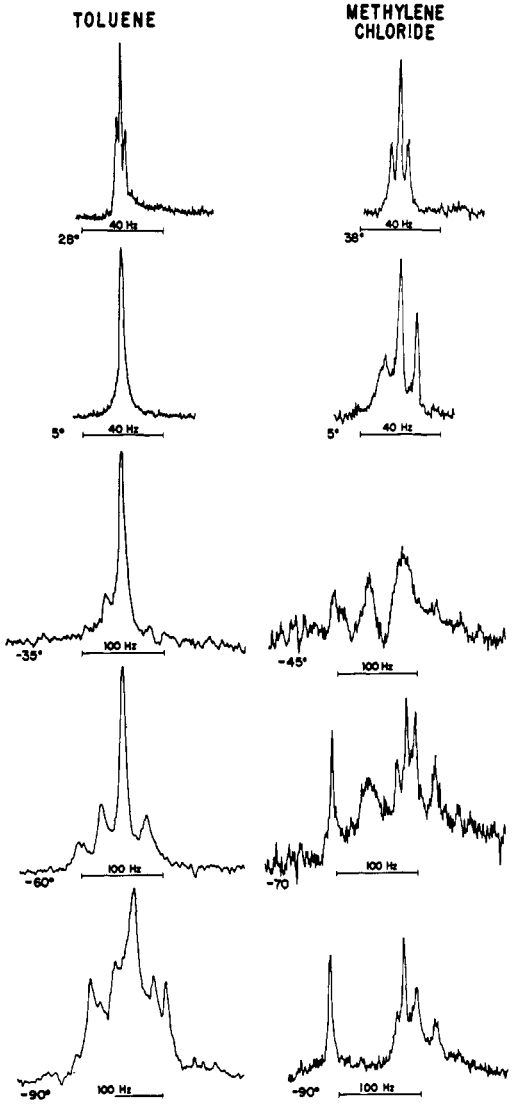

Figure 8. Temperature dependence of the hydride region ^1H (90 MHz) nmr spectra for $HIr(CO)_2[P(C_6H_5)_3]_2$ taken in toluene and methylene chloride solvents.

arrangement but this may partly reflect interactions with the rather polar solvent ($CHClF_2$) or inaccuracies in the temperature measurements. Since the value obtained for $\Delta G^{\ddagger}$ is relatively insensitive to temperature errors, the value for $\Delta G^{\ddagger}$ (7.25 kcal mol^{-1}) is taken as an estimate of the barrier to rearrangement in $HRh[P(OC_2H_5)_3]_4$.

The hydride region proton nmr spectra of several other transition metal hydrides of the type HML_4 have been measured in a variety of solvents. In all cases, a high-temperature limit quintet (doublet of quintets where M = Rh) was observed. The only change that took place on cooling was a gradual broadening of the spectrum which can be attributed to increasing viscosity. In several cases the nature of the phosphorus ligand, L, is such that the solubility of the complex is too low in chlorodifluoromethane or chlorodifluoromethane–methylene chloride mixtures for spectral studies below about $-110°$. The high-temperature limit nmr parameters are given in Table II, together with an estimate for the upper limits to the free energies of activation consistent with the observed spectra assuming a C_{3v} geometry with reasonably large differences between the H–P axial and H–P equatorial coupling constants. It is possible, but unlikely, that some complexes have a tetragonal prismatic geometry with four equivalent phosphorus atoms.

$HIr(CO)_2(PR_3)_2$ Complexes. Nmr Data and Solution Structure. In a recent publication, Yagupsky and Wilkinson[11] described the preparation and temperature-dependent ir and nmr spectra of several hydrides of the type $HIr(CO)_2(PR_3)_2$. The spectra were interpreted in terms of an equilibrium between two isomers, A and B, with an exchange rate which is low for the nmr time scale at low temperatures ($-70°$ in carbon disulfide) and high at room temperatures. The equilibrium for $HIr(CO)_2[P(C_6H_5)_3]_2$ was studied in a wide range of solvents. In the high-temperature limit, the hydride region nmr spectrum of the triphenylphosphine derivative was a sharp triplet with an averaged coupling constant. The coupling constant is dependent upon both temperature and solvent (Figure 8 and also Figure 2 of ref 11) and may in some cases be zero. The temperature and solvent dependence of this coupling constant was interpreted as a change in relative concentrations of the species A and B as the temperature and solvent were varied leading to a different weighted averaging of the coupling constants. On cooling, the first spectral change observed is attributed to a change in relative concentrations of A and B. On further cooling, the rate of exchange becomes comparable to the nmr chemical shift separations between the isomers. The nmr spectra broaden, and line-shape changes occur which depend on the rate of exchange between A and B and upon their relative concentrations. Unfortunately, the solubility of the triphenylphosphine derivative is too low in most solvents to effectively explore the low-temperature region. Yagupsky and Wilkinson[11] described the low-temperature limit spectra in CS_2 at $-70°$, as the superposition of two triplets, τ 20.98, J = 19 Hz (A), and τ 21.6, J = 35 Hz (B), of rela-

tive intensity 2:1; the data which we present below indicate that this is not the true low-temperature limit. The details of the low-temperature spectra in toluene-d_8 are somewhat obscured by viscosity broadening. In methylene chloride the spectra are quite sharp at $-90°$ and indicate that the low-temperature limit has not been reached (Figure 8). The spectrum at $-70°$ in methylene chloride only crudely approximates two triplets. The central line of one of the triplets is quite broad. This line becomes broader on lowering the temperature over the range -60 to $-80°$ while the width of the other lines in the spectrum is relatively unaffected.

To overcome the problems associated with the low solubility of the triphenylphosphine derivative, the more soluble tri-*p*-tolylphosphine analog, $HIr(CO)_2[P(p\text{-}C_7H_7)_3]_2$, was prepared. The left side of Figure 9 shows the temperature-dependent hydride region proton nmr spectrum of the tolyl derivative (1:1 CH_2Cl_2–$CHClF_2$). The spectrum at $-120°$ consists of the superposition of a triplet and a doublet of doublets corresponding to the two different isomers, A and B. As the temperature is increased from $-120°$ (Figure 9), the proportion of isomer A increases. At the same time, the outer lines of the doublet of doublets, representing isomer B, broaden due to an intramolecular exchange process which equilibrates phosphorus environments within the isomer. The observation that the outer lines broaden rather than the inner lines indicates that the two H–P coupling constants in B are of opposite sign. On further warming, the two outer lines continue to broaden and eventually begin to coalesce into a broad line between the two inner lines of the low-temperature doublet of doublets. At the same time the relative concentration of isomer A is increasing but the triplet lines are still sharp. At $-70°$, the spectrum looks like two overlapping triplets except that the central line for one of the triplets (isomer B) is broader than the other lines in the spectrum. Also, the triplet of isomer A has started to broaden due to the nonmutual intramolecular exchange process A $\rightleftharpoons$ B. As the temperature is raised still further, the whole spectrum broadens and then sharpens to a triplet. The high-temperature limit cannot be attained in 50% CH_2Cl_2–50% $CHClF_2$ due to the low boiling point of the solvent mixture but can be observed in other solvents (CH_2Cl_2, toluene, etc.). Since the averaged coupling constant observed in the high-temperature triplet is much less than that corresponding to the average value for isomer B, the sign of the H–P coupling constant in isomer A must be of opposite sign to the large H–P coupling constant in B. (The low-temperature spectra between -120 and $-70°$ indicate that the coupling constants themselves are not significantly temperature dependent.) Consequently, the relative signs of the three coupling constants can be determined.

In Figure 10, all possible trigonal-bipyramidal structures are depicted for an $HIr(CO)_2(PR_3)_2$ composition. Yagupsky and Wilkinson[11] suggest that isomer A has structure **1** and isomer B structure **2**. Isomers **1**, **2**, and **5** would yield a triplet proton spectrum and isomers **3** and **4** a doublet of doublets. We note that the crystal structure of $HIr(CO)_2[P(C_6H_5)_3]_2$ shows isomer **3** to be the only isomer present in the solid state.[20] This in

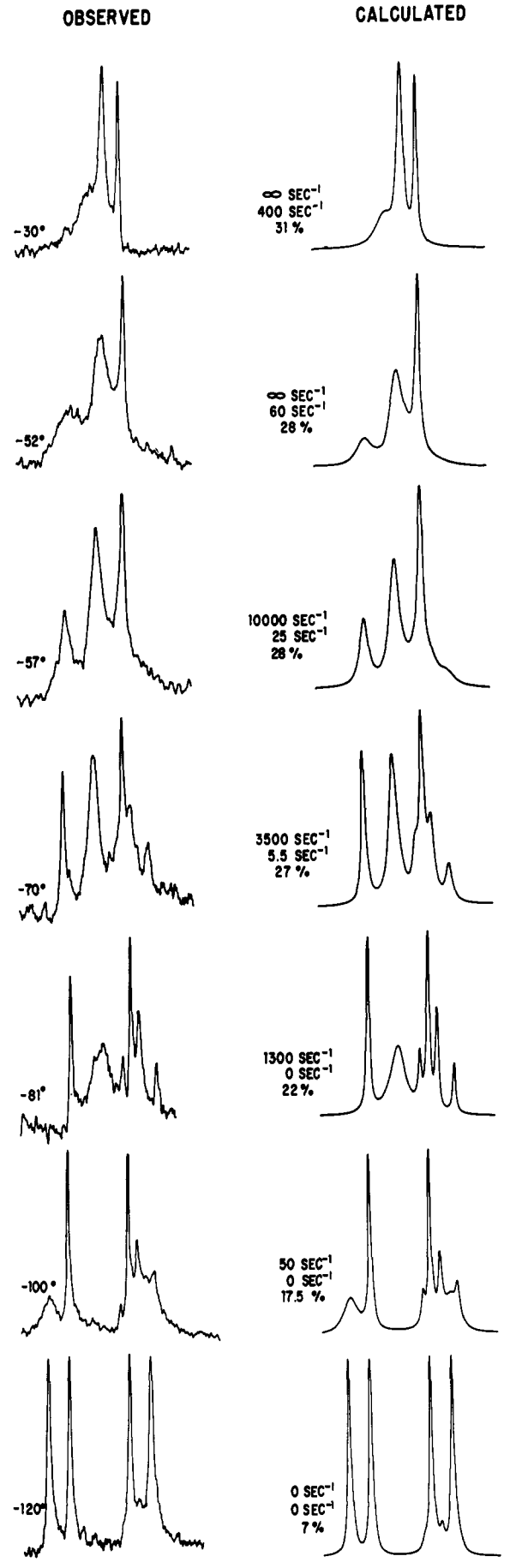

Figure 9. Observed and calculated hydride region ^1H (90 MHz) nmr spectra for $HIr(CO)_2[P(p\text{-tolyl})_3]_2$ in 50% $CHClF_2$–50% CH_2Cl_2.

(20) M. Ciechanowicz, A. C. Skapski, and P. G. H. Troughton, *Acta Crystallogr., Sect. A*, **25**, S172 (1969).

Table III. Nmr Parameters for the Isomers of Complexes of the Type $HIr(CO)_2L_2$

		Isomer A		Isomer B	
		δ_A[a]	J_{HP}	δ_B[a]	$J_{HP_{av}}$
$HIr(CO)_2[P(C_6H_5)_3]_2$	CH_2Cl_2	10.67	∓18.5	11.18	±35.5
$HIr(CO)_2[P(C_6H_5)_3]_2$	Toluene	10.14	∓17.5	10.20	±35.0
$HIr(CO)_2[P(p\text{-tolyl})_3]_2$	Toluene	10.11	∓19.5	10.07	±34.0
$HIr(CO)_2[P(p\text{-tolyl})_3]_2$	50% CH_2Cl_2–50% $CHClF_2$	10.79	∓19.5	11.29	±34.0

[a] Parts per million upfield from TMS.

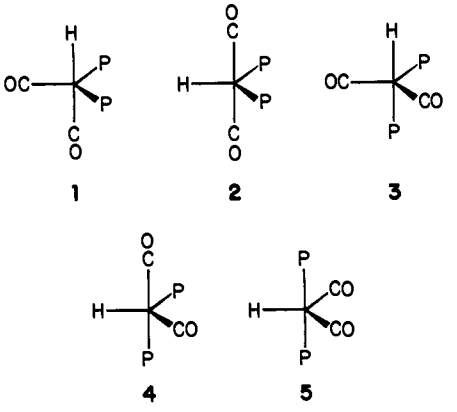

Figure 10. Possible trigonal-bipyramidal isomers for $HIr(CO)_2L_2$ molecules.

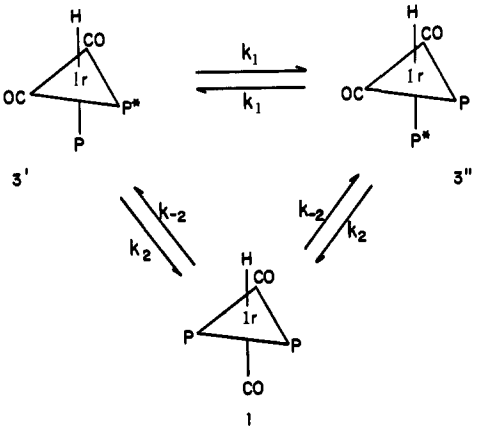

Figure 11. Model used in the interpretation of the hydride region ^1H (90 MHz) nmr spectra for the $HIr(CO)_2L_2$ systems.

itself does not establish isomer **3** as the solution species giving rise to the doublet of doublets because isomer **3** might be present in *solution* in too low a concentration to be detected by the nmr measurement and might be the least soluble isomer. Under such conditions, isomer **4** might be the isomer that gives rise to the doublet of doublets. We note, however, that in cases where the *ligating nuclei alone* reasonably define a trigonal bipyramid, all five-coordinate transition metal hydrides that have been investigated by X-ray analysis[21] have been shown to have the hydrogen nucleus at an axial position. We presume that this reflects a favorable electronic factor in transition metal, five-coordinate stereochemistry. Furthermore, if the ligands other than hydrogen are bulky, the placement of hydrogen at an axial position can lead to minimum nonbonding repulsions by allowing the central metal nucleus to move out of the equatorial plane "away" from the hydrogen atom. This consideration lends credence to the assignment of structure **1** and **3** to the isomers A and B, respectively. This is further supported by solution infrared studies reported by Yagupsky and Wilkinson.[11] For one isomer of $HIr(CO)_2[P(C_6H_5)_3]_2$ there is strong coupling between the Ir–H and the one CO stretching vibration as demonstrated by deuteration studies. Structure **1** best accounts for these data. We further note that in second or third row transition metal hydrides the $|J_{HP}|$ value is substantially larger where the HMP angle approaches 180° than where it is ~90°. The observed J_{HP} values are ∓19.5 Hz for the isomer represented by the triplet and ±92 Hz and ∓24 Hz for the one represented by the doublet of doublets. The near identity of the triplet separation with the smaller separation in the doublet of doublets argues for a close angular HMP relationship in both isomers. For the two isomers, **3** and **4**, that have inequivalent phosphorus nuclei, this would require the pairing of **1** with **3** or **1** with **4**. The large difference in coupling constants for the isomer yielding a doublet of doublets argues for a structure with near 90° HMP and 180° HMP angles, *i.e.*, isomer **3**. The evidence in total strikes us as being overwhelmingly in favor of isomers **1** and **3**.

The temperature-dependent nmr spectra can now be interpreted in terms of the equilibria shown in Figure 11. The stimulated spectra shown in Figure 9 are calculated on the basis of the three-site exchange model corresponding to the three species, **1**, **3'**, and **3''**. At the higher temperatures where the process **3'** ⇌ **3''** becomes very fast, the line shapes do not depend on the precise value of this rate and for the purposes of our calculations the rate may be set equal to infinity. In this case the problem simplifies to a two-site exchange problem with a triplet nmr spectrum at each site. As can be seen from Figure 9, good agreement is obtained between calculated and observed spectra at all temperatures. The spectra were simulated holding the chemical shifts and coupling constants fixed at their low-temperature limit values. The four parameters ($k_1 = k_{-1}$), k_2, k_{-2}, and T_2 (assumed to have the same value at each site) were then varied to give a good visual fit to the observed spectra. The nmr parameters obtained from the low-temperature limit spectra are: **1**, δ = 10.79 ppm upfield from TMS, J = ∓19.5 Hz; **3**, δ = 11.29 ppm upfield from TMS, $J_{HP_{ax}}$ = ±92 Hz, $J_{HP_{eq}}$ = ∓24 Hz. In other solvents we have been able to obtain only the averaged value of $J_{HP_{ax}}$ and $J_{HP_{eq}}$. The results are given in Table III.

For the mutual exchange process, $\Delta G^{\pm}$ (183°K) = 8.4 kcal mol^{-1}. For the process **1** → **3**, $\Delta G^{\pm}$ (223°K)

(21) B. A. Frenz and J. A. Ibers, "The Hydride Series," Vol. I, E. L. Muetterties, Ed., Marcel Dekker, New York, N. Y., 1971, Chapter III.

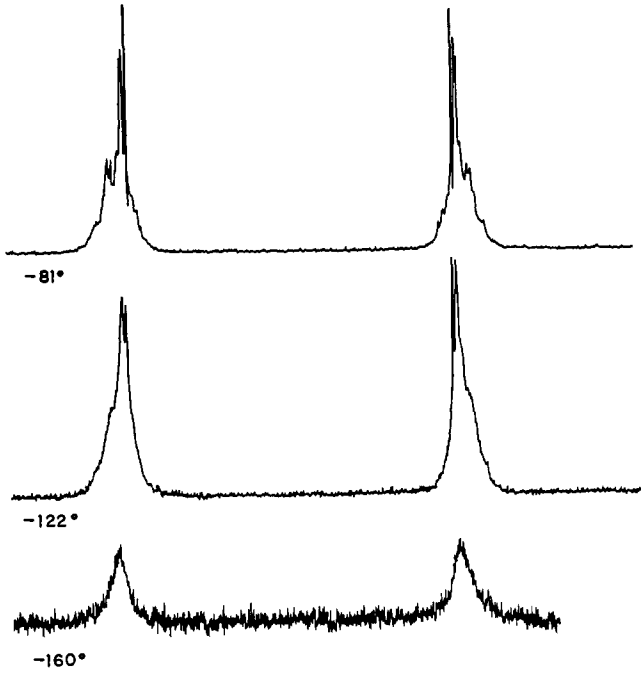

Figure 12. ^{19}F (84.66 MHz) nmr spectra for $Fe(PF_3)_5$ in $CHClF_2$ taken at three temperatures.

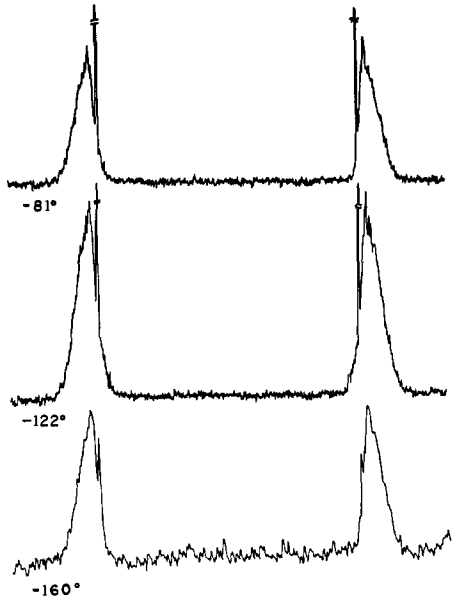

Figure 13. ^{19}F (84.66 MHz) nmr spectra for $Ru(PF_3)_5$ in $CHClF_2$ taken at three temperatures.

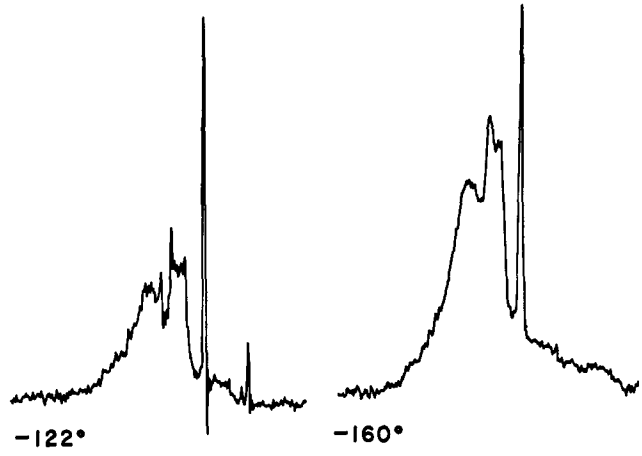

Figure 14. Downfield half of the ^{19}F (84.66 MHz) nmr spectra for $Os(PF_3)_5$ in $CHClF_2$ taken at two temperatures.

= 11.0 kcal mol^{-1}. For the equilibrium **1** ↔ **3**, K = (**1**)/(**3**), ΔG is small (less than 800 cal/mol^{-1}). Unfortunately, the equilibrium data obtained from the lineshape analysis (Figure 9) are not accurate enough for ΔH and ΔS to be separately determined.

The above analysis of the temperature-dependent spectra in 1:1 CH_2Cl–$CHClF_2$ facilitates the interpretation of the hydride region nmr spectra in other solvents and of the triphenylphosphine derivative in a variety of solvents. The spectra of the triphenylphosphine derivative in methylene chloride (Figure 8) are very similar to those shown in Figure 9 except that the low-temperature limit cannot be attained. Similarly, although the temperature-dependent hydride region nmr spectra of the tri-*p*-tolylphosphine and triphenylphosphine derivatives in toluene do not have a close resemblance to the spectra shown in Figure 9, they may still most reasonably be interpreted in terms of the model depicted in Figure 11. Observed and simulated spectra (based on the model shown in Figure 11) are in good agreement. The somewhat different appearance of the spectra in toluene is due to (a) broader lines at low temperature due to viscosity effects; (b) the chemical shift separation of the two isomers **1** and **3** is smaller in toluene; and (c) the fraction of the less polar isomer **1** is larger in toluene (~40% at −75°).

Infrared and nmr evidence has been reported for the presence of two isomers in solution for $HCo(CO)_2[P(n\text{-}C_4H_9)_3]_2$.[22] We agree with this general conclusion and have extended the nmr measurements to lower temperatures (−160° in $CHClF_2$); however, we have been unable to observe limiting slow exchange spectra. It is probable that the isomers involved have the same form as those discussed above for the iridium systems, rather than the ones proposed by Pregaglia, *et al.*[22]

(22) C. F. Pregaglia, A. Andreetta, G. F. Ferrari, and R. Ugo, *J. Organometal. Chem.*, 30, 387 (1971).

In any event, the rearrangement and isomerization barriers appear to be substantially lower in the cobalt case.

$Fe(PF_3)_5$, $Ru(PF_3)_5$, and $Os(PF_3)_5$. The ^{19}F (84.66 MHz) nmr spectra of $Fe(PF_3)_5$, $Ru(PF_3)_5$, and $Os(PF_3)_5$ in $CHClF_2$ at several temperatures are shown in Figures 12–14. These spectra are very similar to the high-temperature limit ^{19}F nmr spectra of the $HM(PF_3)_4$ complexes (Figures 1–3) except that there is no ^{19}F–^1H coupling. They may be partially analyzed in a similar fashion (*vide supra*) in terms of five PF_3 groups equivalent on the nmr time scale. In this case, the separation of the sharp inner lines is $|J_{FP} + 4J_{FP'}|$; and since there are no F–H or F–M couplings, there is no additional resolved fine structure. As for the $HM(PF_3)_4$ systems, the appearance of the ^{19}F spectra requires that $J_{FP} \gg J_{FP'}$, $J_{PP'}$, $J_{FF'}$, and that J_{FP} and $J_{FP'}$ are of opposite sign (the sharp lines are sharp inner lines rather than sharp outer lines). On cooling to −160° the only change observed in the spectra is a gradual broadening of the lines presumably due to increasing viscosity. There is no indication that the ex-

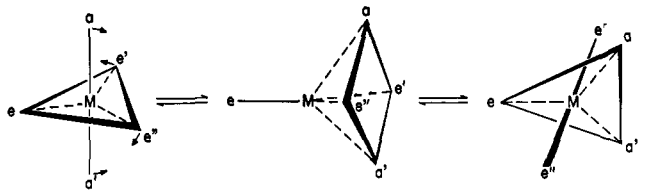

Figure 15. Schematic representation of the Berry mechanism with depiction of the square-pyramidal transition state. In one rearrangement, the two axial nuclei exchange positions with two of the equatorial nuclei.

change process has been lowered to a rate comparable to the nmr time scale, and we conclude that in all three cases the barrier to intramolecular rearrangement is less than 5 kcal mol^{-1}. To date, the limiting slow exchange spectra for a pentacoordinate molecule or ion with five identical ligands have not been detected.[2] The nmr parameters are given in Table IV.

Table IV. ^{19}F Nmr Parameters of the $M(PF_3)_5$ Systems[a] in $CHClF_2$ Solutions

Compound	Temp, °C	δ	$\lvert J_{PF} + 4J_{PF'}\rvert$, Hz
$Fe(PF_3)_5$	−81	74.04	1218
$Ru(PF_3)_5$	−81	74.23	1209
$Os(PF_3)_5$	−122	55.11	1250

[a] The chemical shift is measured in parts per million from the upfield component of $CHClF_2$.

Idealized Rearrangement Mechanisms. Intramolecular rearrangement mechanisms may be discussed in the context of permutational character, physical motions, and topological or graphical representations.[23] The permutational mechanism and the physical mechanism should be differentiated and discussed separately because basic permutational mechanisms can be rigorously and exhaustively delineated[14] but physical mechanisms cannot.

An intramolecular rearrangement permutes nuclear positions, and two or more nuclei may be permuted per rearrangement step. The permutational character of a rearrangement is especially relevant to nmr studies of such phenomena because the line-shape changes (assuming the jump model) provide only information about the nuclear permutations which convert the initial labeled configuration into a new configuration. Unfortunately, for many five-coordinate molecules of interest there are no permutational distinctions and therefore no mechanistic information is contained in the nmr line-shape changes. Even in those cases where such data can be obtained, many plausible physical mechanisms may be formulated in consistency with each permutational mechanism. Specifically for trigonal-bipyramidal geometry, there is only one permutational mechanism (in addition to the identity) for C_{3v} XML_4 (see Appendix I). There are two permutational mechanisms for D_{3h} ML_5 and for C_{2v} XML_4. The latter case has been examined by ^{31}P nmr for $(CH_3)_2NPF_4$ and the dominant permutational mechanism was established.[24] Several physical mechanisms, the Berry, the turnstile, and the anti-Berry, have this permutational character; only a few plausible mechanisms were eliminated by this study. Simply because of the small number of ligand nuclei in five-coordination, the nmr approach provides very limited mechanistic information.

In principle, the primary physical motion in a rearrangement may be derived from analysis of vibrational or rotational spectra. In most instances this is not feasible, and it has not been done with rigor in five-coordination. Models proposed to date are largely intuitive projections. In any case, there are limitations to the use of such idealized models. Because of misunderstandings that have arisen with respect to five-coordinate rearrangement models, we pursue this subject in a little greater detail than in our earlier discussions of physical mechanisms.

The Berry mechanism[1] takes specific account of the close relationship of the two most common polytopal forms in five-coordination: the trigonal bipyramid and the square pyramid. A bending mode of a trigonal-bipyramidal molecule that involves the two axial and two equatorial bonds leads to a square-pyramidal form from which it may return to the original configuration or form a new configuration wherein the permutation of two axial for two equatorial atom nuclei has been achieved. This is illustrated in Figure 15. The Berry mechanism is strictly applicable only to trigonal-bipyramidal molecules of D_{3h} symmetry (ML_5 species) and of C_{2v} symmetry (XML_4 species) or to square-pyramidal molecules of C_{4v} symmetry (ML_5 or XML_4 species). With any other point group symmetry in either of the two idealized polytopal forms, the physical motion must depart from the idealized representation. Consider, for example, a trigonal-bipyramidal XML_4 molecule of C_{3v} symmetry. A Berry mechanism for rearrangement in such a molecule requires that the axial X and L nuclei or groups show precisely the same motion. This is highly improbable unless X and L are very similar in electronic character and size. The greater the distinction between X and L the more the motion will depart from a Berry motion and may well approach some other kind of idealized motion and yield a transition state distinct from the square pyramid. The validity of invoking the idealized Berry mechanism becomes questionable as the diversity of ligand nuclei increases and as the angular parameters of the actual molecule depart from the 90 and 120° required for a trigonal bipyramid. If the departure from 90 and 120° for the actual interbond angles is significant, then the utilization of any idealized rearrangement mechanism based on a trigonal bipyramid is meaningless. These general comments apply of course to rearrangement mechanisms for a complex of any coordination number, but they are especially relevant to five-coordination where in actual complexes a number of reaction channels differing little in energy characteristics are available for intramolecular rearrangements.

The Berry mechanism has been used to explicate a large body of exchange data for five-coordinate molecules and reaction intermediates; and it, in conjunction with a crude stereochemical guide, is a model of good

(23) The graphical representations have value for comparisons of physical mechanisms which have different permutational character or, if the connecting line segments are weighted at least qualitatively to represent activation energies, for comparison of physical mechanisms even where the permutational character is the same.

(24) G. M. Whitesides and H. L. Mitchell, *J. Amer. Chem. Soc.*, **91**, 5384 (1969).

predictive value.[2] This success probably reflects the fact that *most* of the five-coordinate molecules (or ions) *considered in this context* have interbond angles relatively close to those for a trigonal bipyramid. Thus even with diverse ligands the dominant intramolecular rearrangement mechanism for a molecule may reasonably resemble in physical motion that for the idealized Berry rearrangement. Nevertheless even if the rearrangement of a five-coordinate molecule or group of molecules can be rationalized satisfactorily by invoking the Berry rearrangement, the actual motion(s) could more closely approach another idealized physical mechanism and traverse transition states of idealized forms other than the square pyramid.

Several mechanisms alternative to the Berry process have been described and all except one are based on a trigonal-bipyramidal ground state. There may be instances where one of these mechanisms may have a higher rate constant than the Berry process especially where the character of the ligands is quite diverse. For certain molecules, some of these alternative mechanisms are of a permutational form distinct from that of the Berry mechanism and in these instances nmr line-shape analysis may provide definitive answers.

One mechanism for rearrangement of five-coordinate complexes which has been proposed as an alternative to the Berry rearrangement is the turnstile rotation.[4] This is permutationally[14] and topologically[3] identical with the Berry mechanism and strictly speaking applies to a trigonal-bipyramidal molecule of D_{3h} or C_s point group symmetry. The turnstile rotation comprises a 180° rotation of one axial and one equatorial ligand as a pair with a 60° rotation, in the same *or* opposite direction of one axial and two equatorial ligands as a trio. In physical motion, the turnstile rotation is distinct from the Berry mechanism and the transition state approximates a C_s form (Figure 16). Like the Berry transition state or intermediate, no interbond angles in the C_s form are defined. Hence, the only distinction between transition states for the two mechanisms is symmetry defined. This distinction is lost once the symmetry of the ground state is not D_{3h} or C_{2v}. Furthermore, although it is not possible to quantify the geometric parameters for the transition states, it is clear they are very similar (this is generally true for idealized five-coordinate forms). Ugi, *et al.*,[4] in presenting arguments for the turnstile rotation over the Berry process have especially emphasized five-coordinate structures which have a tridentate ligand. In some of these cases, the turnstile rotation may well be a low-energy pathway to rearrangement, but it must be kept in mind that cyclic structures are far removed from the D_{3h} and C_{2v} models on which the Berry mechanism was formulated and that the interbond angles may differ substantially from the 90 and 120° required in a trigonal bipyramid. In any case, it appears that the Berry mechanism is much more effective in rationalizing the body of experimental data on molecules with near trigonal-bipyramidal geometry. For example, the near equivalence of activation energies for rearrangement in D_{3h} ML_5 and C_{2v} XML_4 molecules is easily explained with the Berry mechanism but not the turnstile rotation. However, the issue is not adoption of a unique all-encompassing mechanism; the organizational and pedagogical value of the general Berry mechanism in five-coordinate rearrangements is established. An idealized mechanism will be an oversimplification for many five-coordinate molecules, and future mechanism studies should not be limited simply to consideration of one pervasive mechanism. Nmr studies may in some cases limit the types of acceptable mechanisms by establishing the permutational[14] character of the rearrangement. The fine detail of the physical motions will be very difficult to settle, and arguments for or against specific motions will require ancillary information such as infrared and Raman data and structural parameters. This is what we attempt here. In the following sections, we rely upon structural and stereochemical data to invoke new physical rearrangement mechanisms for the five-coordinate complexes of the HML_4 and HML_2L_2' classes. We take note, however, that more than one rearrangement pathway may be utilized because the potential surface in five-coordination is relatively smooth and complex.

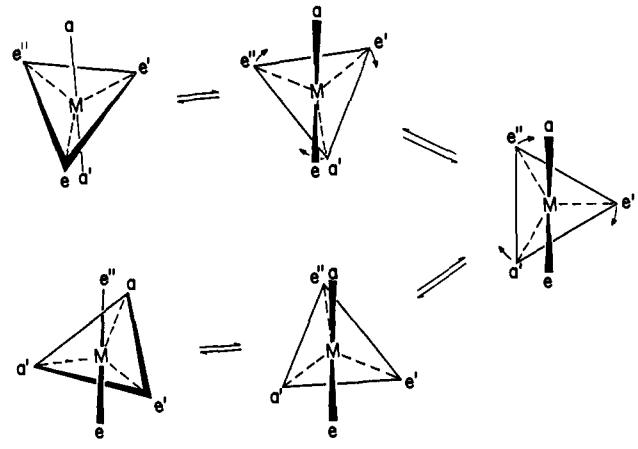

Figure 16. Partial representation of the turnstile rearrangement mechanism. The ea pair may rotate in the same or opposite direction to that of the e'a'e'' triad.

Rearrangement Mechanism for HML_4 Complexes. All HML_4 molecules investigated by X-ray analysis have a near regular tetrahedral ML_4 substructure. These include $HCo(PF_3)_4$,[15] $HCo[P(C_6H_5)(OC_2H_5)_2]_4$,[25] $HRh[P(C_6H_5)_3]_4$,[26] and $HRh[P(C_6H_5)_3]_3[As(C_6H_5)_3]$.[27] The hydrogen bonded to the metal nucleus was located in only one[25] of these X-ray studies; the hydrogen was on a tetrahedral face. In the remaining cases plausible arguments were advanced for a similar placement of the hydrogen atom. Our nmr studies establish a solution structure with C_{3v} symmetry suggesting that the hydrogen is in fact on a tetrahedral face. It seems reasonable that for all HML_4 species in which L is relatively bulky this type of structure will prevail; we therefore distinguish this as a special idealized five-coordinate polytopal form and call it the pseudotetrahedral form.

We have established from the nmr studies that the $HM(PF_3)_4$ (M = Ru, Os, Co, Rh, and Ir) molecules and ions and $HRh[P(OC_2H_5)_3]_4$ are stereochemically nonrigid. The limiting slow and fast exchange spectra were observed and the preservation of HP and/or HF spin coupling in the fast exchange limits shows the exchange to be intramolecular. Since these five-coordinate

(25) D. D. Titus, A. A. Orio, R. E. Marsh, and H. B. Gray, *Chem. Commun.*, 322 (1971).
(26) R. W. Baker and P. Pauling, *ibid.*, 1495 (1969).
(27) R. W. Baker, B. Ilmaier, P. J. Pauling, and R. S. Nyholm, *ibid.*, 1077 (1970).

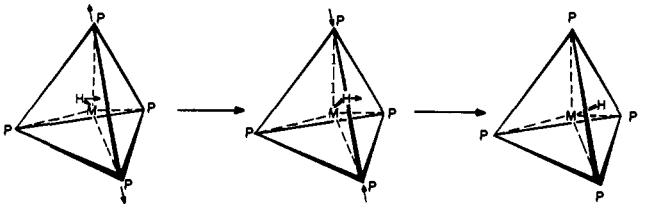

Figure 17. "Tetrahedral tunneling" mechanism. For ease of representation, regular tetrahedra have been used for both the initial state and the transition state. In real molecules there will, in general, be distortions in both cases. It is anticipated that the PMP angle in the plane occupied by the hydrogen atom in the transition state will be larger than the corresponding angle in the initial state (this is indicated by the arrows).

species do not have trigonal-bipyramidal (or tetragonal-pyramidal) geometry, it is meaningless to invoke a Berry mechanism or any other mechanism based on a trigonal-bipyramidal form. We propose that the *lowest* energy path to a rearrangement that equilibrates phosphorus environments in these pseudotetrahedral forms is motion of the hydrogen toward an edge of the tetrahedron with a concomitant MP bending motion that enlarges this tetrahedral edge (Figure 17). The hydrogen atom could then either return to the original face or to a new tetrahedral face. This rearrangement mechanism which we have termed "tetrahedral tunneling" is not simply a hydrogen atom motion as is clearly shown by the very small rate reduction in going from $HRh(PF_3)_4$ to $DRh(PF_3)_4$. The energy required for phosphorus atom motion, necessary for tetrahedral edge elongation as the hydrogen atom goes from one face to another and for adjustment of departures from a regular MP_4 structure in the ground state, may be the major contribution to the barrier.

The regular decrease in rearrangement barrier for a given series with decreasing atomic number of the central nucleus is rather interesting. We suggest that the increased size of the metal atom with increased atomic number may result in an increased departure from the idealized regular tetrahedral ground state. This departure from the idealized case could well raise the rearrangement barrier. The slightly lower barrier for the anionic $HM(PF_3)_4^-$ species than for their neutral analogs may also reflect a closer approach to the regular tetrahedral MP_4 substructure in the former. All other factors being equal, a formal charge should enhance the PF_3–PF_3 repulsions since some fraction of the negative charge should reside on those strongly π-accepting ligands, favoring a more nearly regular tetrahedral MP_4 substructure.

Limiting slow exchange spectra were not observed for $HCo[P(OC_2H_5)_3]_4$. Because the near limiting spectrum was observed for the rhodium analog and because we would expect the pseudotetrahedral form to be favored on going from Rh to Co, we propose that the rearrangement barrier for the cobalt complex is low (<6 kcal/mol). The same conclusion applies to the cationic nickel analog although there are no barrier data for *any* HML_4 species from the nickel triad. The bidentate complexes of rhodium and iridium, $HM[(C_6H_5)_2PCH_2CH_2P(C_6H_5)_2]_2$, should also have near regular tetrahedral MP_4 substructures. The rearrangement barriers are quite low and the linking CH_2CH_2 chains lie closely along only two of the six tetrahedral edges leaving four edges open for the hydrogen atom traverse of tetrahedral faces.

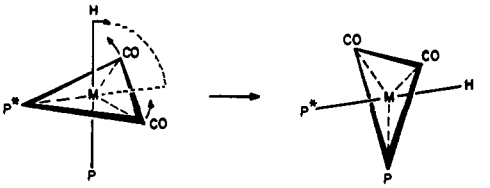

Figure 18. Schematic representation of the process which renders the phosphorus atoms equivalent within isomer **3**.

Rearrangement Mechanism for $HM(CO)_2(PR_3)_2$ Complexes. For $HIr(CO)_2[P(p\text{-}C_7H_7)_3]_2$ in solution we have a unique observation in five-coordination. Two isomers coexist each in substantial concentration—a situation experimentally observed only in a few other cases, $HCo(CO)_2[P(n\text{-}C_4H_9)_3]_2$,[22] $HRu(NO)L_3$,[28] and $CF_3Co(PF_3)_2(CO)_2$,[29]—and one of the two isomers rearranges intramolecularly more rapidly than the two isomers interconvert. This provides important qualitative mechanistic information.

Since the X-ray data show that near trigonal-bipyramidal geometry prevails at least for one isomer, an attempt is made here to accommodate the mechanistic information in a Berry type of rearrangement. Isomer **3** can effect an equilibration of phosphous environments in a single Berry rearrangement step.

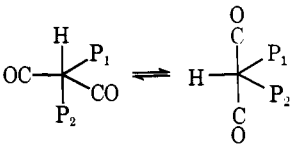

(1)

Interconversion minimally requires two steps.

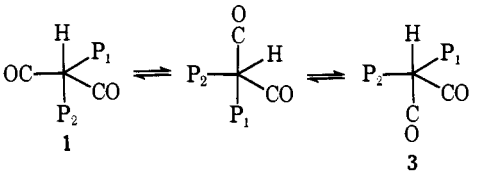

(2)

1 **3**

Without knowing anything about the various rate constants for rearrangement in **3** and for interconversion of **1** and **3**, it is difficult to rationalize the data but it is not implausible that the Berry mechanism is the dominating mechanism for the two processes since the two-step character of interconversion may largely account for the lower rate for this process relative to the one-step process for rearrangement in **1**. However, it is our feeling that any isomer in this series which has the hydrogen at an equatorial position is of much higher energy than those with an axial hydrogen. Accordingly we would anticipate a barrier larger than the 8–10 kcal observed.

We propose an alternative rearrangement process for isomer **3** that consists of a hydrogen motion which brings this nucleus axial to the initially equatorial phosphorus nucleus with a concomitant bending motion of the carbonyl groups. This is outlined in Figure 18.

(28) S. T. Wilson and J. A. Osborn, *J. Amer. Chem. Soc.*, **93**, 3068 (1971).

(29) C. A. Udovich, R. J. Clark, and H. Haas, *Inorg. Chem.*, **8**, 1066 (1969); C. A. Udovich and R. J. Clark, *J. Amer. Chem. Soc.*, **91**, 526 (1969).

This mechanism may be less energetic than a Berry rearrangement. A slightly more activated process, because it requires more M–P bending, in addition to H and CO motion, allows interconversion of **1** and **3**. This is illustrated in Figure 19. The proposed processes have the additional attractive feature that they are true single-step rearrangements. Equilibrium 1 for the Berry mechanism requires the postulation of two discrete intermediates or transition states and equilibrium 2 requires three.

Finally it is instructive to inquire into the reasons underlying the much smaller barriers observed for ML_5 species relative to HML_4 species. Based on idealized trigonal-bipyramidal models, the result could be rationalized by assuming that trigonal bipyramids with the hydride ligand in an equatorial position are much less stable than those with the hydrogen axial. As noted above this appears to be supported by the growing body of X-ray crystal structure information. For structures which are nearer to the pseudotetrahedral form the argument is not so simple, but it would be logical to assume that the difference resides in an unfavorable electronic contribution in the pseudotetrahedral transition state for HML_4 relative to the tetragonal-pyramidal transition state for the Berry process in the ML_5 complexes. A related way of looking at the same problem is discussed in Appendix II.

Acknowledgment. We wish to acknowledge the assistance of Mr. W. Peet for the preparation of the transition metal hydride complexes and Mr. G. Watunya for obtaining some of the nmr spectra.

Appendix I. Permutational Mechanistic Distinctions for Mutual Exchange in Pentacoordination

In a previous publication[14] we carried out a systematic analysis of the basic types of temperature dependence of the nmr line shapes calculated on the basis of a jump model (the basic permutational sets). This type of analysis in terms of the point group of the molecule and the possible permutations of equivalent ligands among themselves can be applied to any mutual exchange process.

In general each basic permutational set leads to a calculated temperature-dependent nmr line-shape behavior distinguishable from those corresponding to other permutational sets although in practice the difference between the line shapes calculated for different permutational sets may be too small to be useful. The observed temperature-dependent nmr line shapes corresponding to any mutual exchange process(es) can be analyzed in terms of one of the basic permutational sets alone or a linear combination of them. Table V shows the results of an analysis of the basic permutational sets for trigonal-bipyramidal systems of the type MX_5, MX_4Y, and MX_3Y_2. In each case the reference labeling is given at the left-hand side of Table V and only one of the several equivalent basic permutational sets of each type is given in cycle form.

In Table VI the basic permutational sets (or linear combinations of them) are assigned to some possible mechanisms. The mechanisms considered are:[1,3,4] (1) Berry mechanism, (2) axial–equatorial exchange, (3) equatorial–equatorial exchange, (4) 2 equatorial–1 axial exchange, (5) D_{5h} reaction intermediate, (6) 2 axial–1 equatorial exchange, (7) turnstile mechanism,

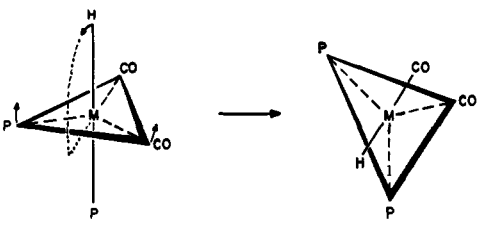

Figure 19. Schematic representation of the process which equilibrates isomers **1** and **3**.

Table V

Molecule	Point group	Order of permutational group	Basic sets[a]
	D_{3h}	5!	A (15)(24) B (15)(23) (14)(35) (12)(35) (14)(25) (14)(23) (25)(34) (13)(24) (15)(34) (13)(25) (24)(35) (12)(34)
	C_{3v}	4!1!	A (14)(32) (12)(34) (13)(24)
	C_{2v}	4!1!	A (25)(34) B (25) (24)(35) (35) (24) (34)
	C_{2v}	3!2!	A (35) (34)
	C_s	3!2!	A (24) B (15) C (24)(15) (34) (34)(15)

[a] Excluding the identity.

Table VI. Assignment of Basic Permutation Sets of Some Physical Mechanisms in Five-Coordinate Complexes

MX_5 (D_{3h})	3	E
	1, 7, 8	A
	2, 4, 6	B
	5	A + B + 3E
MX_4Y (C_{3v})	3	E
	2, 4, 6	A
	5	A + 3E
MX_4Y (C_{2v})	3, 5	E
	1, 7, 8	A
	2, 4, 6	B
	5	E, A + 2E
MX_3Y_2 (C_{2v})	3	E
	2, 6	A
	5	E, A + 2E
MX_3Y_2 (C_s)	3	E
	2, 4, 6	A
	2, 4	B
	1, 7, 8	C
	5	A + E, C + 2E

(8) anti-Berry mechanism. The anti-Berry mechanism consists of the pairwise exchange of an axial ligand and an equatorial ligand and of another axial ligand with another equatorial ligand. We consider in Table VI processes involving only one trigonal-bipyramidal isomer.

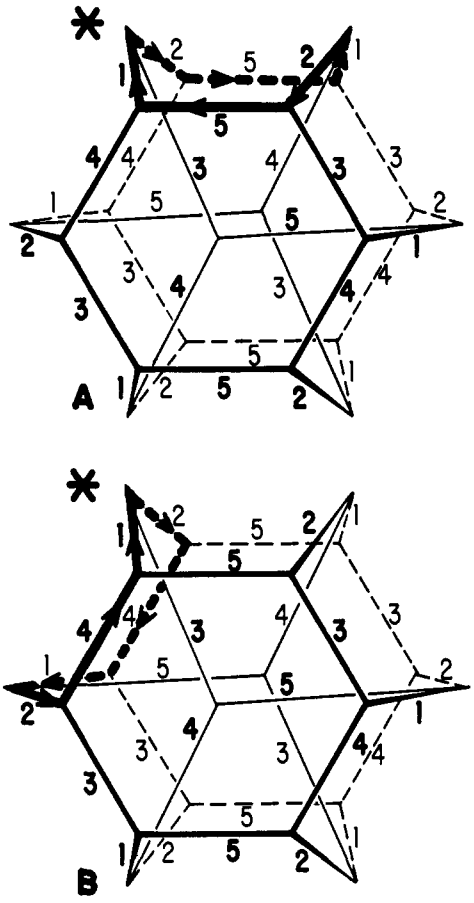

Figure 20. Desargues–Levi graph[31] for the Berry rearrangement process. The vertices represent equilibrium configurations and the edges represent Berry type rearrangements. The numbers indicate the pivotal ligand.

Appendix II. Barriers to Intramolecular Rearrangement in Five-Coordinate Complexes

There is, at this time, no known ML_5 complex with D_{3h} symmetry in which the barrier to intramolecular rearrangement is sufficiently high that it can be estimated using the nmr line-shape method.[2] This observation places an upper limit of about 5 kcal mol^{-1} on the barrier height in such complexes. By contrast the barriers restricting intramolecular rearrangement in C_{3v} molecules of the type XML_4 are frequently greater than 5 kcal mol^{-1}. This result is rationalized below in terms of the symmetry of the barriers restricting the rearrangement process. For a D_{3h} ML_5 system there are 20 distinct equilibrium configurations[30] (equivalent energy minima) which can be interconverted by means of a Berry process[1] *via* the 30 distinct C_{4v} transition states (30 equivalent energy maxima corresponding to the 30 possible configurations for a C_{4v} ML_5 system). In Figure 20 the set of 20 equilibrium configurations and 30 reaction paths is depicted in the form of a Desargues–Levi graph[31] in which the equilibrium configurations are represented by vertices and the exchange paths by edges. The labeling on the edges in Figure 20 corresponds to the pivotal[2,3] ligand.

The shortest route by which a particular configuration can return to itself by a series of Berry-type processes involves six steps (a cycle of six steps). In this

(30) E.L. Muetterties, *Inorg. Chem.*, 6, 635 (1967).
(31) K. Mislow, *Accounts Chem. Res.*, 3, 321 (1970).

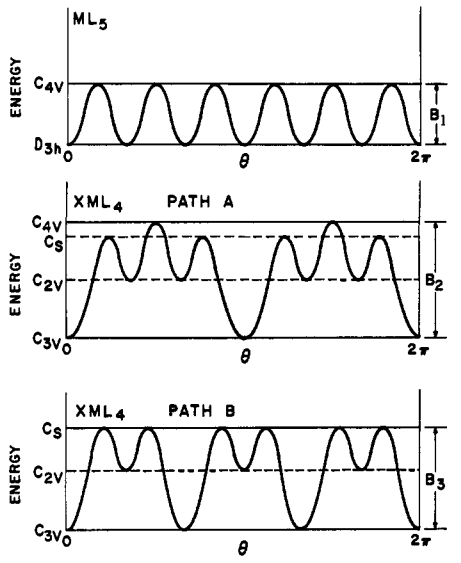

Figure 21. Idealized potential energy functions for Berry type rearrangement in D_{3h} ML_5 and C_{3v} MXL_4 complexes.

case all six steps[3] are equivalent and there are six equivalent energy maxima and minima (Figure 21). The barrier to rearrangement can be written in terms of a reaction coordinate θ (which indicates the progress of the rearrangement process through a cycle) as

$$V_1(\theta) = \frac{V_6}{2}(1 - \cos 6\theta) + \frac{V_{12}}{2}(1 - \cos 12\theta) + \ldots \quad (1)$$

For an XML_4 system of C_{3v} symmetry there are only eight equivalent configurations (the remaining 12 correspond to the C_{2v} configurations in which X is equatorial). Consequently the edges and vertices of the Desargues–Levi graph shown in Figure 20 are now no longer all equivalent. However, it can still be used to depict the possible nonidealized Berry-type rearrangement processes. Starting with the arbitrary equilibrium configuration

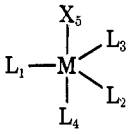

(indicated by * in Figure 20)

and using L_2 as the pivotal ligand for the first step, two distinct six-step cycles can be constructed.

Cycle A contains the steps $C_{3v} \rightarrow C_{2v} \rightarrow C_{2v} \rightarrow C_{3v} \rightarrow C_{2v} \rightarrow C_{2v} \rightarrow C_{3v}$ where the trigonal-bipyramidal configurations with X equatorial and axial are represented by their corresponding point groups. The barrier to rearrangement for cycles of type A is shown in Figure 21 and may be written

$$V_2(\theta) = \frac{V_2}{2}(1 - \cos 2\theta) + \frac{V_4}{2}(1 - \cos 4\theta) + \frac{V_6}{2}(1 - \cos 6\theta) + \ldots$$

Cycle B contains the steps $C_{3v} \rightarrow C_{2v} \rightarrow C_{3v} \rightarrow C_{2v} \rightarrow C_{3v} \rightarrow C_{2v} \rightarrow C_{3v}$. In this case the barrier can be written

$$V_3(\theta) = \frac{V_3}{2}(1 - \cos 3\theta) + \frac{V_6}{2}(1 - \cos 6\theta) + \ldots$$

A potential function of this type is shown in the last line of Figure 21.

It is reasonable to suppose that the barriers to rearrangement *can* be much higher for the XML_4 complex than for the ML_5 since in the former case twofold terms in the potential function may be nonzero for cycle A and threefold terms may be nonzero for cycle B. In general, highly periodic barriers are observed to be low, and this idea has been found to be useful in consideration of barriers to internal rotation and barriers to pseudorotation in small cyclic systems.

In the case of an XML_4 complex with X equatorial and with C_{2v} symmetry, the barriers have the same form as those shown in rows 2 and 3 of Figure 21; consequently, the barrier can be high. However, in the case of path A with the minima at $\pi/3$, $2\pi/3$, $4\pi/3$, and $5\pi/3$ (corresponding to X in an axial position) now lower than those at 0, π, and 2π (X equatorial), the chemical shifts and coupling constants can be averaged by a Berry-type process which exchanges the molecule between the equilibrium configurations at approximately $\pi/3$ and $2\pi/3$ and between those at approximately $4\pi/3$ and $5\pi/3$ with X as the pivotal ligand. Consequently the full barrier need not be overcome and since θ changes by only about $\pi/3$ in the exchange process the effective barrier should be low. This seems to be the case with the exception of systems in which the X–M bond has partial double bond character.[2,32,33] In the case of an X_2ML_3 system with the two X ligands equatorial (C_{2v} symmetry) θ must change by $\sim 2\pi/3$, at least, in order to reach another equivalent potential energy minimum and a large barrier can be anticipated. The above discussion was confined to complexes undergoing a Berry type of motion. However, because of the large number of equivalent energy minima for ML_5 systems, the barrier to rearrangement is expected to have a higher periodicity and consequently *may* have a smaller magnitude than for similar X_nML_{5-n} systems in cases where the rearrangement mechanism is different.

(32) F. N. Tebbe and E. L. Muetterties, *Inorg. Chem.*, 7, 172 (1968).
(33) E. L. Muetterties, P. Meakin, and R. Hoffmann, *J. Amer. Chem. Soc.*, in press.

Hindered Rotation in Trimethylsilyl Amides

A. Komoriya and C. H. Yoder*

Contribution from the Department of Chemistry, Franklin and Marshall College, Lancaster, Pennsylvania 17604. *Received October 19, 1971*

Abstract: Rotational barriers were determined for *N-tert*-butylformamide (I) and *N*-trimethylsilylformamide (II) in chlorobenzene by the total line-shape procedure. Barriers for *N*-methyl-*N*-trimethylsilylformamide and -acetamide were obtained by an approximate method. The free energy of activation for II extrapolated to infinite dilution is 3 kcal/mol lower than that for I. A rationalization based on the (p–d)π model is offered. Isomer ratios were measured for all compounds. Activation parameters for bis(trimethylsilyl)acetamide were also determined by the total line-shape procedure and compared with those of the mono derivatives.

While the effect of third period atoms on inversion processes at nitrogen and phosphorus has recently been investigated,[1] their effect on the rotational process in the classical amide system has received little attention. We present here the results of an investigation of the rotational barriers in a series of trimethylsilyl amides. These compounds, some of which have been used extensively as silylating agents,[2] are also interesting from a structural standpoint. The monotrimethylsilyl amides, such as *N*-methyl-*N*-trimethylsilylacetamide, are generally conceded to have the silyl group attached to nitrogen.[2b] The bis derivatives, on the other hand, have been reported as *N,N*-bis(trimethylsilyl)-substituted amides (**1**)[2b] and as *N,O*-bis(trimethylsilyl)-substituted imidates (**2**).[3] Both types

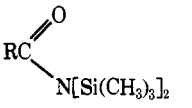

1

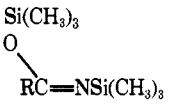

2

of compounds, mono and bis substituted, exhibit temperature dependent nmr spectra which could be ascribed to either hindered rotation about the C–N bond or exchange of trimethylsilyl groups.

The present work, then, is an attempt to (a) determine the effect of *N*-trimethylsilyl substitution on the rotational barrier in amides and (b) lay the groundwork for a more rigorous examination of the structure of bis(silyl) amides and related compounds.

Experimental Section

Compounds. Bis(trimethylsilyl)acetamide was obtained from the reaction of trimethylchlorosilane with acetamide according to the procedure of Klebe, *et al.*,[4] bp 50° (11 mm) [lit.[4] 71–73° (35 mm)]. Trimethylsilylacetamide was prepared from the reaction of equi-

(1) H. Kessler, *Angew. Chem., Int. Ed. Engl.*, 9, 219 (1970); R. D. Baechler and K. Mislow, *J. Amer. Chem. Soc.*, 92, 4758 (1970); S. J. Brois, *ibid.*, 90, 506 (1968); J. D. Andose, J.-M. Lehn, K. Mislow, and J. Wagner, *ibid.*, 92, 4050 (1970); F. A. L. Anet, R. D. Trepka, and D. J. Cram, *ibid.*, 89, 357 (1967), and references therein.
(2) (a) J. F. Klebe, *Accounts Chem. Res.*, 3, 299 (1970); (b) L. Birkofer and A. Ritter, *Angew. Chem., Int. Ed. Engl.*, 4, 417 (1965).
(3) C. Krüger, E. G. Rochow, and U. Wannagat, *Chem. Ber.*, 96, 2138 (1963); J. Pump and E. G. Rochow, *ibid.*, 97, 627 (1964).
(4) J. F. Klebe, H. Finkbeiner, and D. M. White, *J. Amer. Chem. Soc.*, 88, 3390 (1966).